talloporphyrin made these weak orbital interactions less favorable. The impact of axial ligands on the conformations of the spin-labeled high-spin iron(III) complexes appears to be analogous to that which was observed for the Cu(II) and Ag(II) complexes.

1,3,5-Trinitrobenzene (TNB) forms a π complex with a pyrrole ring of FeTTPCl.[32,33] The spectrum of the iron signal for Fe(III)F in the presence of 5 equiv of TNB (Figure 4B) has a larger fraction of the intensity of the $g_\perp$ signal at $g \sim 6$ than was observed in toluene solution (Figure 4A). This indicates that complexation with TNB results in a larger population of the conformations with weaker spin-spin interaction. Complexation with TNB also favored the conformations with weaker spin-spin interaction for Fe(P)X, P = I, II, and IV-VII, X = F^- and Cl^-. Addition of TNB to the samples had little impact on the EPR spectra of VIII-XI or $Fe(P)(DMSO)_2^+$, P = I-VII.

Formation of π complexes with the porphyrin ring has been shown to influence the electronic structure of porphyrins.[34] For example, complexation of Fe(TPP)X with TNB decreases the affinity of the iron for axial ligands.[32] Also, interaction of one molecule of toluene with the porphyrin ring of $Mn(TPP)(H_2O)^+$ caused an increase in the length of the Mn-O bond to the coordinated water.[34] The decrease in the populations of conformations with stronger spin-spin interaction for Fe(P)X, P = I-VII, caused by formation of the TNB complexes again suggests that these conformations have weak orbital interactions between the ortho substituent and the porphyrin π orbitals or the metal orbitals.

NMR studies of Fe(TTP)X have shown that aggregation via π complexation between two porphyrin rings is significant in 5-30 mM solutions at -30 °C.[33] The concentration dependence of the EPR spectra of Fe(P)X between 0.1 and 10 mM was examined to check for effects of aggregation. The line widths in the spectra of VIII-XI increased as the concentration increased, but the spectra were otherwise unchanged. For Fe(P)X, P = I-VII, X = F^-, Cl^-, and Br^-, the line widths and the populations of the conformations with weaker spin-spin interaction increased as the concentration increased. It is proposed that the porphyrin-porphyrin π complexation influenced the conformational equilibria analogous to the effect of TNB complexation.

These spin-labeled iron porphyrin complexes have provided examples of iron-nitroxyl spin-spin interaction ranging from less than the line widths of the spectra to $|J| = 0.17$ cm^{-1}. This set of complexes has greatly expanded the range of demonstrated electron-electron spin-spin couplings in EPR spectra. The variety of conformations observed for these complexes precludes a correlation between molecular structure and the strength of the interaction. Complexes with rigid geometries are needed to provide those correlations.

Acknowledgment. The partial support of this work by NIH Grant GM21156 is gratefully acknowledged. Purchase of the IBM ER200 EPR spectrometer was funded in part by NSF Grant CHE8411282.

(32) Kabbani, A. T.; LaMar, G. N.; *J. Magn. Reson.* **1981**, *43*, 90.
(33) Snyder, R. V.; LaMar, G. N. *J. Am. Chem. Soc.* **1977**, *99*, 7178.
(34) Williamson, M. M.; Hill, C. *Inorg. Chem.* **1987**, *26*, 4155 and references therein.

Contribution from the Department of Chemistry, The University of North Carolina, Chapel Hill, North Carolina 27514, and United States Geological Survey, Reston, Virginia 22092

Synthesis and Spectral and Redox Properties of Three Triply Bridged Complexes of Ruthenium

Antoni Llobet,[1a,b] Maria E. Curry,[1a] Howard T. Evans,[1c] and Thomas J. Meyer*[,1a]

Received July 22, 1988

Syntheses are described for the ligand-bridged complexes $[(tpm)Ru^{III}(\mu\text{-}O)(\mu\text{-}L)_2Ru^{III}(tpm)]^{n+}$ (L = $O_2P(O)(OH)$, n = 0 (**1**); L = O_2CO, n = 0 (**2**); L = O_2CCH_3, n = 2 (**3**); tpm is the tridentate, facial ligand tris(1-pyrazolyl)methane. The X-ray crystal structure of $[(tpm)Ru(\mu\text{-}O)(\mu\text{-}O_2P(O)(OH))_2Ru(tpm)]\cdot 8H_2O$ was determined from three-dimensional X-ray counter data. The complex crystallizes in the trigonal space group $P3_221$ with three molecules in a cell of dimensions a = 18.759 (4) Å and c = 9.970 (6) Å. The structure was refined to a weighted R factor of 0.042 based on 1480 independent reflections with $I \geq 3\sigma(I)$. The structure reveals that the complex consists of two six-coordinate ruthenium atoms that are joined by a μ-oxo bridge (r_{Ru-O} = 1.87 Å; ∠RuORu = 124.6°) and two μ-hydrogen phosphato bridges (average r_{Ru-O} = 2.07 Å) which are capped by two tpm ligands. The results of cyclic voltammetric and coulometric experiments show that the complexes undergo both oxidative and reductive processes in solution. Upon reduction, the ligand-bridged structure is lost and the monomer $[(tpm)Ru(H_2O)_3]^{2+}$ appears quantitatively. All three complexes are diamagnetic in solution. The diamagnetism is a consequence of strong electronic coupling between the low-spin d^5 Ru(III) metal ions through the oxo bridge and the relatively small Ru-O-Ru angle.

Introduction

Of the μ-oxo complexes of ruthenium, the structurally characterized examples include (1) complexes such as $[(bpy)_2(L)Ru^{III}(O)Ru^{III}(L)(bpy)_2]^{4+}$ (L = H_2O, NO_2^-), in which there is a μ-oxo link between two Ru(III) sites,[2] (2) the triangular, planar structure in $[Ru_3O(L)_3(O_2CCH_3)_6]$ (L = H_2O, PPh_3), where the oxo group bridges three ruthenium ions, each pair of which is bridged by three acetate ligands,[3] and (3) ruthenium red $[Ru_3O_2(NH_3)_{14}]^{6+}$ and its analogues, which contain the oligomeric group N-Ru-O-Ru-O-Ru-N.[4]

From the results of previous studies, the μ-oxo link in compounds of Ru can sustain strong electronic coupling between the metal sites. The coupling can lead to significant modifications in the chemical and physical properties of the resulting materials

(1) (a) The University of North Carolina. (b) Fulbright "La Caixa" fellow, Barcelona, Spain. Permanent address: Departament de Química (Area 10), Universitat Autònoma de Barcelona, 08193 Bellaterra, Barcelona, Spain. (c) U.S. Geological Survey.
(2) (a) Phelps, D. W.; Kahn, E. M.; Hodgson, D. J. *Inorg. Chem.* **1975**, *14*, 2486. (b) Gilbert, J. A.; Eggleston, D. S.; Murphy, W. R.; Geselowitz, D. A.; Gersten, S. W.; Hodgson, D. J.; Meyer, T. J. *J. Am. Chem. Soc.* **1985**, *107*, 3855.
(3) (a) Cotton, F. A.; Norman, J. G. *Inorg. Chim. Acta* **1972**, *6*, 411. (b) Spencer, A.; Wilkinson, G. *J. Chem. Soc., Dalton Trans.* **1972**, 1570. (c) Cotton, F. A.; Norman, J. G.; Spencer, A.; Wilkinson, G. *J. Chem. Soc., Dalton Trans.* **1971**, 967.
(4) (a) Carrondo, M. A. A. F. d. C. T.; Griffith, W. P.; Hall, J. P.; Skapski, A. C. *Biochim. Biophys. Acta* **1980**, *627*, 332. (b) Smith, P. M.; Fealey, T.; Earley, J. A.; Silverton, J. V. *Inorg. Chem.* **1971**, *10*, 1943. (c) Geselowitz, D. A.; Wlodzimierz, K.; Meyer, T. J. *Inorg. Chem.* **1986**, *25*, 2015.

0020-1669/89/1328-3131$01.50/0

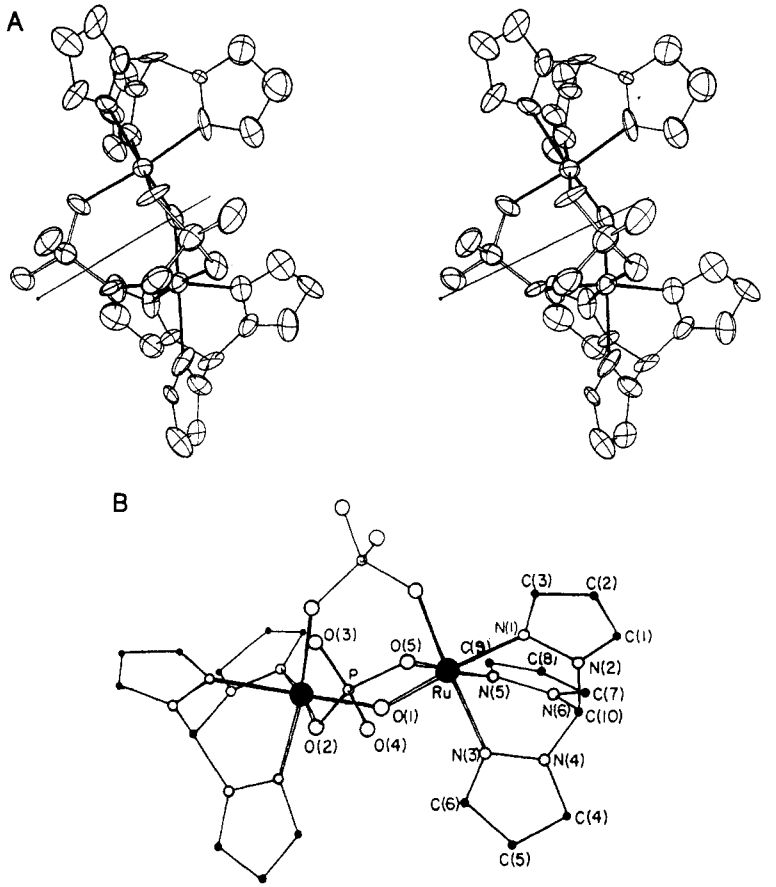

Figure 1. (A) View of the ligand-bridged molecule $[(tpm)Ru(\mu\text{-}O)(\mu\text{-}O_2P(O)(OH))_2Ru(tpm)]$. The halves of the molecule are related by a crystallographic 2-fold symmetry axis that runs through the bridging oxygen atom. (B) Diagram showing the labeling scheme used for the atoms.

when compared to those of related monomers. Another important characteristic of such compounds is the accessibility of higher oxidation states.[2b,4c,5] The accessibility of higher oxidation states has been shown to lead to a versatile stoichiometric and/or catalytic oxidative chemistry toward a variety of inorganic and organic substrates.[2b,5b-d] This reactivity is reminiscent of the reactivity properties of related oxo complexes of Ru(IV).[6] Of particular note, upon oxidation, the (μ-oxo)ruthenium ion $[Ru_2O(H_2O)_2(bpy)_4]^{4+}$ is capable of acting as a catalyst for the oxidation of water to oxygen[2b,7] or of chloride to chlorine.[5d,8] From a biological point of view, ruthenium red is used to stain selectively and thereby provides a basis for the visualization of the structure of cell walls.[9a] It is known to bind to a wide variety of materials,[9b] including isolated DNA,[9c] and it also interferes with the binding and transport of Ca^{2+} in mitochondria.[9d,e]

We have been investigating the underlying μ-oxo chemistry of ruthenium based on the tridentate facial ligand tris(1-pyrazolyl)methane (tpm). In previous papers,[10] we have developed

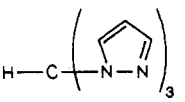

tpm

the synthetic chemistry of ruthenium tpm based complexes of the type $[(tpm)(4,4'\text{-}(L)_2\text{-}bpy)RuX]^{n+}$ (L = H, CH_3, Ph, NH_2, $COOCH_2CH_3$; X = Cl^-, H_2O, O^{2-}, pyridine) and have studied their physical and chemical properties. During the course of our synthetic work with aqua tpm complexes, we have encountered tribridged complexes that have a Ru–O–Ru bridge. In these complexes $O_2P(O)(OH)^{2-}$, O_2CO^{2-}, or $O_2CCH_3^-$ groups act as additional bridging ligands. We report here on the structural and chemical properties of the multiply bridged complexes.

Experimental Section

Materials. All reagents were ACS grade and were used without further purification. Elemental analyses were performed by Galbraith Laboratories, Knoxville, TN.

Preparations. $[(tpm)RuCl_3]\cdot 1.5H_2O$ was prepared as previously described.[10a]

(μ-Oxo)bis(μ-hydrogen phosphato)bis(tris(1-pyrazolyl)methane)diruthenium(III)–5.5-Water, $[(tpm)Ru(\mu\text{-}O)(\mu\text{-}O_2P(O)(OH))_2Ru(tpm)]\cdot$

(5) (a) Weaver, T. R.; Meyer, T. J.; Adeyemi, S. A.; Brown, G. M.; Eckberg, R. P.; Hatfield, W. E.; Johnson, E. C.; Murray, R. W.; Untereker, D. *J. Am. Chem. Soc.* **1975**, *97*, 3039. (b) Doppelt, P.; Meyer, T. J. *Inorg. Chem.* **1987**, *26*, 2027. (c) Raven, S.; Meyer, T. J. *Inorg. Chem.* **1988**, *27*, 4478. (d) Vining, W. J.; Meyer, T. J. *Inorg. Chem.* **1986**, *25*, 2023. Vining, W. J.; Meyer, T. J. *J. Electroanal. Chem. Interfacial Electrochem.* **1985**, *195*, 183.

(6) (a) Moyer, B. A.; Thompson, M. S.; Meyer, T. J. *J. Am. Chem. Soc.* **1980**, *102*, 2310. Thompson, M. S.; De Giovani, W. F.; Moyer, B. A.; Meyer, T. J. *J. Org. Chem.* **1984**, *49*, 4972. (b) Thompson, M. S.; Meyer, T. J. *J. Am. Chem. Soc.* **1982**, *104*, 4106. Thompson, M. S.; Meyer, T. J. *J. Am. Chem. Soc.* **1982**, *104*, 5070. (c) Meyer, T. J. *J. Electrochem. Soc.* **1984**, *131*, 221C. (d) Che, C.-M.; Wong, K.-Y.; Mak, T. C. W. *J. Chem. Soc., Chem. Commun.* **1985**, 988. Che, C.-M.; Cheng, W.-K.; Mak, T. C. W. *J. Chem. Soc., Chem. Commun.* **1986**, 200. (e) Roecker, L.; Meyer, T. J. *J. Am. Chem. Soc.* **1986**, *108*, 4066. Roecker, L.; Meyer, T. J. *J. Am. Chem. Soc.* **1987**, *109*, 746. (f) Marmion, M. E.; Takeuchi, K. J. *J. Am. Chem. Soc.* **1986**, *108*, 510. (g) Marmion, M. E.; Takeuchi, K. J. *J. Chem. Soc., Chem. Commun.* **1987**, 1396. (h) Bailey, C. L.; Drago, R. S. *J. Chem. Soc., Chem. Commun.* **1987**, 179. (i) Lau, T. C.; Kochi, J. K. *J. Chem. Soc., Chem. Commun.* **1987**, 798. (j) Wong, K.-W.; Che, C.-M.; Anson, F. C. *Inorg. Chem.* **1987**, *26*, 737. Che, C.-M.; Lai, T.-F.; Wong, K.-Y. *Inorg. Chem.* **1987**, *26*, 2289.

(7) Gersten, S. W.; Samuels, G. J.; Meyer, T. J. *J. Am. Chem. Soc.* **1982**, *104*, 4029.

(8) Ellis, C. D.; Gilbert, J. A.; Murphy, W. R.; Meyer, T. J. *J. Am. Chem. Soc.* **1983**, *105*, 4842.

(9) (a) Blanquet, P. R. *Histochemistry* **1976**, *47*, 63. (b) Luft, J. H. *Anat. Rec.* **1971**, *171*, 347. (c) Hanke, D. E.; Northcote, D. H. *Biopolymers* **1975**, *14*, 1. (d) Moore, C. L. *Biochem. Biophys. Res. Commun.* **1971**, *42*, 298. (e) Vasington, F. D.; Gazzotti, P.; Tiozzo, R.; Carafoli, E. *Biochim. Biophys. Acta* **1972**, *256*, 43.

(10) (a) Llobet, A.; Doppelt, P.; Meyer, T. J. *Inorg. Chem.* **1988**, *27*, 514. (b) Barqawi, K.; Llobet, A.; Meyer, T. J. *J. Am. Chem. Soc.* **1988**, *110*, 7751.

5.5H_2O (1). A 200-mg sample of [(tpm)$RuCl_3$]·1.5H_2O was added to 100 mL of a 0.1 M, pH 7 phosphate buffer solution. The mixture was allowed to stand at room temperature for 3 days, during which an intense blue color appeared. The remaining solid was filtered and the volume of the filtrate reduced by placing the filtered solution in an open vessel at 35 °C for several days until a crystalline dark blue solid was formed. The crystals were collected, washed with a small amount of cold water, and dried under a vacuum; yield 160 mg, 71.9%. ^1H NMR (D_2O): δ 9.3 (d, 2, J_{12} = 2.7 Hz, H1), 8.7 (d, 2, J_{23} = 1.9 Hz, H3), 8.3 (d, 4, J_{45} = 2.7 Hz, H4), 7.1 (double d, 2, H2), 6.3 (double d, 4, J_{56} = 1.9 Hz, H5), 5.8 (d, 4, H6). Anal. Calcd for $C_{20}H_{33}N_{12}O_{13.5}P_2Ru_2$: C, 25.61; H, 3.52; N, 17.92. Found: C, 25.93; H, 3.86; N, 17.57.

(μ-Oxo)bis(μ-carbonato)bis(tris(1-pyrazolyl)methane)diruthenium(III)-12-Water, [(tpm)Ru(μ-O)(μ-O_2CO)$_2$Ru(tpm)]·12H_2O (2). The carbonato-bridged complex was prepared in a manner analogous to that reported for **1** but with a 0.1 M sodium carbonate solution instead of a 0.1 M phosphate solution; yield 130 mg, 58.5%. ^1H NMR (D_2O): δ 9.1 (d, 2, J_{12} = 2.7 Hz, H1), 8.9 (d, 2, J_{23} = 1.9 Hz, H3), 8.4 (d, 4, J_{45} = 2.7 Hz, H4), 7.1 (double d, 2, H2), 6.3 (double d, 4, J_{56} = 1.9 Hz, H5), 5.8 (d, 4, H6). Anal. Calcd for $C_{22}H_{44}N_{12}O_{19}Ru_2$: C, 26.88; H, 4.48; N, 17.10. Found: C, 26.61; H, 4.14; N, 16.77. The ^1H NMR assignments for this complex and for complexes described subsequently are keyed to the crystal structure shown in Figure 1. The hydrogen atoms have been tagged in agreement with the corresponding carbon atoms. The protons in the two equivalent pyrazolyl rings are labeled H4, H5, H6 and H7, H8, H9, whereas those in the third ring are labeled H1, H2, H3 (see Figure 1).

(μ-Oxo)bis(μ-acetato)bis(tris(1-pyrazolyl)methane)diruthenium(III) Hexafluorophosphate-8.5-Water, [(tpm)Ru(μ-O)(μ-O_2CCH_3)$_2$Ru(tpm)](PF_6)$_2$·8.5H_2O (3). A 200-mg sample of [(tpm)$RuCl_3$]·1.5H_2O was added to 100 mL of a 0.1 M sodium acetate solution. The mixture was allowed to stand at room temperature for 3 days until the solution was an intense blue. The remaining solid was removed by filtration. Addition of a few drops of a saturated solution of potassium hexafluorophosphate caused the precipitation of the desired complex as a blue solid. The solid was collected, washed with a small amount of cold water, and dried under a vacuum: yield 167.9 mg, 61.5%. ^1H NMR (acetone-d_6): δ 10.8 (s, 2, H10), 9.7 (d, 2, J_{12} = 2.7 Hz, H1), 9.1 (d, 2, J_{23} = 1.9 Hz, H3), 8.9 (d, 4, J_{45} = 2.7 Hz, H4), 7.4 (double d, 2, H2), 6.6 (double d, 4, J_{56} = 1.9 Hz, H5), 6.2 (d, 4, H6), 1.9 (s, 6, CH_3). Anal. Calcd for $C_{24}H_{43}N_{12}O_{13.5}P_2F_{12}Ru_2$: C, 23.86; H, 3.56; N, 13.92. Found: C, 23.48; H, 3.12; N, 13.40.

Measurements. Cyclic voltammetric measurements were carried out by using a PAR Model 173 potentiostat/galvanostat or a PAR 264A polarographic analyzer/stripping voltammeter. Coulometric measurements were made by using a PAR Model 179 digital coulometer. The cyclic voltammetric measurements utilized a Teflon-sheathed glassy-carbon disk (1.5-mm radius) as a working electrode, a platinum wire as the auxiliary electrode, and a saturated calomel reference electrode (SSCE) in a one-compartment cell. The concentration of the complexes was approximately 1 mM, and unless explicitly specified, the scan rate was carried out at 100 mV/s. The pH measurements were made with a Radiometer pHM62 pH meter. All $E_{1/2}$ values reported in this work were estimated from cyclic voltammetry as the average of the oxidative and reductive peak potentials, $(E_{p,a} + E_{p,c})/2$. UV–visible spectra were recorded by using a Hewlett-Packard Model 8451A UV–vis diode-array spectrophotometer with 1-cm quartz cells. The ^1H NMR spectra were recorded on an IBM AC-200 spectrometer. IR spectra were recorded in KBr pellets on a Nicolet 2000 FT-IR instrument.

X-ray Crystallography. A deep blue irregularly shaped prism of [(tpm)Ru(μ-O)(μ-$O_2P(O)(OH)_2$)Ru(tpm)] of approximate dimensions 0.1 × 0.1 × 0.2 mm was used for data collection on an Enraf-Nonius CAD4 diffractometer employing Mo Kα radiation and a graphite monochromator. Precession photographs indicated the existence of the noncentrosymmetric trigonal space group $P3_221$ or $P3_121$. Lattice parameters were obtained at 19 °C by a least-squares fit of the angular settings of 25 reflections and are listed along with other experimental data in Table I. The intensities and angular settings of three standard reflections, monitored frequently throughout the data collection process, showed no systematic variations over the collection period. Details of the procedures for data collection and reduction have been described previously.[11]

A Patterson map was used to find the ruthenium atoms, and an electron density map revealed the positions of all non-hydrogen atoms in the molecule. Refinement in $P3_221$ by least-squares analysis in the last stages with full-matrix, isomorphous extinction and anisotropic thermal parameters for all atoms (based on data weighted by I/σ from counting statistics) led to the final reliability indices shown in Table I. Dispersion corrections were included in the data analysis, but absorption corrections were not because of the small coefficient (μ = 8.0 cm^{-1}). No evidence of the hydrogen atoms could be found in the difference maps, and they were not included in the calculations. Atomic scattering factors for non-hydrogen atoms and dispersion factors for the ruthenium and phosphorus atoms were taken from ref 12.

In order to test the choice between enantiomorphic space groups, the structure was also refined in the space group $P3_121$. Groups of 41 reflections to which ruthenium makes the greatest contribution were compared to the two structures. For $P3_121$ R_w = 0.038, while for $P3_221$ R_w = 0.034, which supports the latter as the appropriate space group.

Five different water molecules were found in the intermolecular region between the μ-oxo complexes. Two lie on the 2-fold axis. In this analysis there should be eight H_2O molecules per formula unit, although some of the sites may not be fully occupied. Two of the sites have very high thermal motions and are only weakly resolved.

The positional parameters for the non-hydrogen atoms derived from the final least-squares cycle, along with their standard deviations esti-

Table I. Crystallographic Data for [(tpm)Ru(μ-O)(μ-$O_2P(O)(OH)$)$_2$Ru(tpm)]·8H_2O

formula	$Ru_2P_2N_{12}O_{17}C_{20}H_{38}$
fw	981.7
system, space group	trigonal, $P3_121$ or $P3_221$
a, Å	18.759 (4)
c, Å	9.970 (6)
V, Å^3	3035
Z	3
d(calcd), g cm^{-3}	1.609
d(obsd), g cm^{-3}	1.61
cryst dimens, mm	0.1 × 0.1 × 0.2
range of data, deg	$0 < 2\theta < 45$
no. of reflns measd	1983 (1480 independent)
no. of reflns used	1098 ($I > 3\sigma(I)$)
radiation, Å	Mo Kα, 0.7107
corrections	Lorentz–polarization extinction, dispersion, no abs
R	0.056
R_w	0.042
temp, °C	19

Table II. Atomic Positional Parameters for [(tpm)Ru(μ-O)(μ-$O_2P(O)(OH)$)$_2$Ru(tpm)]·8H_2O

atom	x	y	z
Ru	0.52709 (9)	0.62687 (9)	0.46624 (15)
O(1)	0.6232 (8)	0.6232	0.5
P	0.4789 (3)	0.4643 (3)	0.3058 (5)
O(2)	0.5037 (8)	0.5541 (7)	0.2991 (10)
O(3)	0.3891 (7)	0.4178 (8)	0.3475 (13)
O(4)	0.4832 (9)	0.4295 (8)	0.1730 (11)
O(5)	0.5257 (8)	0.4487 (7)	0.4181 (12)
N(1)	0.4207 (12)	0.6382 (10)	0.4304 (14)
N(2)	0.4347 (9)	0.7167 (10)	0.4354 (13)
N(3)	0.5502 (10)	0.7089 (10)	0.6199 (12)
N(4)	0.5389 (8)	0.7740 (9)	0.5957 (13)
N(5)	0.5895 (9)	0.7285 (9)	0.3481 (14)
N(6)	0.5765 (10)	0.7931 (10)	0.3592 (14)
C(1)	0.3615 (16)	0.7103 (18)	0.4221 (17)
C(2)	0.3039 (13)	0.6321 (13)	0.4081 (19)
C(3)	0.3434 (11)	0.5885 (14)	0.4137 (17)
C(4)	0.5546 (13)	0.8253 (14)	0.7018 (23)
C(5)	0.5714 (13)	0.7814 (16)	0.8072 (24)
C(6)	0.5708 (13)	0.7109 (13)	0.7484 (16)
C(7)	0.6178 (13)	0.8524 (13)	0.2741 (21)
C(8)	0.6625 (12)	0.8278 (14)	0.1992 (18)
C(9)	0.6421 (13)	0.7505 (14)	0.2485 (22)
C(10)	0.5140 (13)	0.7876 (12)	0.4624 (21)
O(6)	0.7701 (15)	0.7701	0.5
O(7)	0.6684 (13)	0.6684	0.0
O(8)	0.4915 (9)	0.6004 (10)	0.0286 (12)
O(9)	0.3093 (22)	0.2958 (18)	0.1167 (30)
O(10)	0.8807 (34)	0.9621 (54)	0.1255 (50)

(11) Graves, B. J.; Hodgson, D. J. *Acta Crystallogr., Sect. B* **1982**, *B38*, 135.

(12) Hamilton, W. C., Ibers, J. A., Eds. *International Tables for X-Ray Crystallography*; Kynoch Press: Birmingham, England, 1974; Vol. III, Table 3.3.1A.

mated from the inverse matrix, are presented in Table II. Listings of anisotropic thermal parameters for non-hydrogen atoms, and of observed and calculated structure factors are available as supplementary material. All computations were made with the XTAL system.[13]

Results and Discussion

In aqueous solution at room temperature, reactions occur between [(tpm)$RuCl_3$] and the anions in 0.1 M phosphate, carbonate, and acetate solutions to give intense blue solutions that contain the tribridged ions **1**, **2**, and **3**, respectively. In the case of phosphate the balanced reaction is shown in (1).

$$2[(tpm)RuCl_3] + 2HPO_4^{2-} + H_2O \rightarrow [(tpm)Ru(\mu\text{-}O)(\mu\text{-}O_2P(O)(OH))_2Ru(tpm)] + 2H^+ + 6Cl^- \quad (1)$$

General Comments and Description of the Structure of [(tpm)Ru(μ-O)(μ-O_2P(O)(OH))$_2$Ru(tpm)]. The structure of [(tpm)Ru(μ-O)(μ-O_2P(O)(OH))$_2$Ru(tpm)]·8H_2O consists of the neutral, ligand-bridged molecule [(tpm)Ru(μ-O)(μ-O_2P(O)-(OH))$_2$Ru(tpm)], which is surrounded by eight water molecules. The geometry of the complex is illustrated in Figure 1. The halves are related by the 2-fold axis that runs through the bridging oxygen atom. The ruthenium centers are approximately octahedrally coordinated with each metal linked to one tpm ligand, two oxygen atoms from the hydrogen phosphato bridging ligands, and the bridging oxide. Bond lengths and angles are listed in Table III. The same basic molecular framework has already been found for manganese, iron, and vanadium complexes with the tris(1-pyrazolyl)borate anion as facial, tridentate ligands and with acetate as the bidentate bridging ligand. For manganese and iron similar complexes have been described with the cyclic triamine 1,4,7-triazacyclononane as the facial tridentate ligand.[14a-f] Ito and co-workers have reported the X-ray structure of the closely related cation [$(py)_3$Ru(μ-O)(μ-$O_2CCH_3)_2$Ru$(py)_3]^{2+}$ (py = pyridine).[14g] The geometry at the Ru(III) ions in this structure is closely related to the geometry at Ru(III) found in our structure.

The Ru–O–Ru angle in [(tpm)Ru(μ-O)(μ-O_2P(O)-(OH))$_2$Ru(tpm)] is 124°. This is nearly equivalent to the 122° angle found in the structure of the [$(py)_3$Ru(μ-O)(μ-CH_3-$(OO)_2$Ru$(py)_3]^{2+}$ cation. The Ru–O–Ru angle is 165° in the cation [$(bpy)_2(H_2O)$RuORu$(H_2O)(bpy)_2]^{4+}$ and 157° in [$(bpy)_2(NO_2)$RuORu$(NO_2)(bpy)_2]^{2+}$ (bpy = 2,2′-bipyridine). In both cases it is clear from the crystal structure that further bending along the Ru–O–Ru angle is restricted by bpy–bpy steric repulsions. For the μ-oxo dinitro dimer the interplanar separation between the bpy rings, 3.4 Å, is essentially at the van der Waals distance.

In Table IV are collected bond angles and other important molecular dimensions for a series of μ-oxo Ru molecules. For the high-oxidation-state d^4–d^4 ion $[Cl_5Ru^{IV}ORu^{IV}Cl_5]^{4-}$, the geometry at the Ru–O–Ru bridge is linear.[15] Linearity and near-linearity are also observed for the two Ru–O–Ru groups in the mixed-valence, Ru(III)–Ru(IV)–Ru(III) ion Ru-red. However, for the Ru(III)–Ru(III) cases there is a marked propensity toward bending along the Ru–O–Ru axis, which in the limit reaches 120° in [$Ru_3O(O_2CCH_3)_6(PPh_3)_3$].[3a] Strictly speaking, including this triangular cluster in such a comparison is inappropriate. There is expected to be extensive charge delocalization among the three ruthenium ions in the cluster.

Table III. Principal Bond Lengths and Angles in [(tpm)Ru(μ-O)(μ-O_2P(O)(OH))$_2$Ru(tpm)]·8H_2O,[a]

Distances (Å)			
Ru–O(1)	1.868 (15)	C(1)–C(2)	1.32 (4)
Ru–O(2)	2.057 (11)	C(4)–C(5)	1.46 (4)
Ru–O(5)	2.074 (11)	C(7)–C(8)	1.36 (4)
Ru–N(1)	2.139 (25)	C(2)–C(3)	1.35 (4)
Ru–N(3)	2.058 (15)	C(5)–C(6)	1.44 (4)
Ru–N(5)	2.039 (14)	C(8)–C(9)	1.39 (4)
P–O(2)	1.508 (14)	C(3)–N(1)	1.26 (2)
P–O(5)	1.538 (15)	C(6)–N(3)	1.33 (2)
P–O(3)	1.517 (12)	C(9)–N(5)	1.31 (3)
P–O(4)	1.496 (13)	C(10)–N(2)	1.44 (2)
N(1)–N(2)	1.36 (3)	C(10)–N(4)	1.47 (3)
N(3)–N(4)	1.36 (3)	C(10)–N(6)	1.52 (3)
N(5)–N(6)	1.35 (3)	Ru–Ru	3.310 (3)
Angles (deg)			
Ru–O(1)–Ru	124.7 (4)	N(2)–C(10)–N(4)	106 (2)
Ru–N(1)–N(2)	114.6 (1.2)	N(2)–C(10)–N(6)	110 (2)
Ru–N(3)–N(4)	118.0 (1.0)	N(4)–C(10)–N(6)	109 (2)
Ru–N(5)–N(6)	120.9 (1.2)	O(5)–Ru–N(5)	171.6 (7)
Ru–N(1)–C(3)	136.1 (1.9)	O(1)–Ru–N(1)	176.8 (4)
Ru–N(3)–C(6)	133.3 (1.8)	O(2)–Ru–N(3)	173.8 (6)
Ru–N(5)–C(9)	136.1 (1.8)	N(1)–Ru–N(5)	86.5 (7)
Ru–O(2)–P	123.3 (6)	O(1)–Ru–O(5)	97.0 (5)
Ru–O(5)–P	132.6 (7)	N(1)–Ru–O(5)	85.1 (6)
N(1)–N(2)–C(1)	106 (2)	O(1)–Ru–N(5)	91.4 (5)
N(3)–N(4)–C(4)	115 (2)	O(2)–Ru–N(1)	91.7 (6)
N(5)–N(6)–C(7)	114 (2)	O(2)–Ru–N(5)	89.1 (5)
C(1)–C(2)–C(3)	107 (2)	O(2)–Ru–O(1)	90.6 (5)
C(4)–C(5)–C(6)	109 (2)	O(2)–Ru–O(5)	91.4 (5)
C(7)–C(8)–C(9)	105 (2)	N(3)–Ru–N(1)	84.8 (7)
C(2)–C(3)–N(1)	109 (2)	N(3)–Ru–N(5)	85.6 (6)
C(5)–C(6)–N(3)	107 (2)	N(3)–Ru–O(1)	92.7 (6)
C(8)–C(9)–N(5)	112 (2)	N(3)–Ru–O(5)	93.3 (5)
C(3)–N(1)–N(2)	109 (2)	O(2)–P–O(5)	111.4 (7)
C(6)–N(3)–N(4)	109 (2)	O(3)–P–O(4)	105.8 (7)
C(9)–N(5)–N(6)	103 (2)	O(2)–P–O(3)	107.0 (9)
		O(2)–P–O(4)	113.2 (7)
		O(3)–P–O(5)	105.0 (7)
		O(4)–P–O(5)	113.8 (9)

[a] The numbering scheme is shown in Figure 1B.

For the hydrogen phosphato bridged complex **1**, the Ru–O–Ru angle is 124°. This angle is achieved at the cost of compromising structural demands at the bridging ligands. For the coordinated phosphate oxygens O(2) and O(5) the angle O–P–O is 111.4°. The same angle for the noncoordinated phosphate oxygens O(3) and O(4) is 105.8°. This fact suggests that the phosphate bridging ligand is playing a role in the bending along the Ru–O–Ru axis. This bending has a small effect on the Ru–O bond distances at the Ru–O–Ru group when compared to the other Ru(III)–Ru(III) examples in Table IV. The bending does significantly decrease the Ru–Ru separation to a distance of 3.312 Å. At that distance an important factor may be a direct through-space interaction between the Ru ions.[18]

A basis for rationalizing the bending along the Ru–O–Ru axis for the Ru(III)–Ru(III) cases is available from simple MO arguments.[5a,c] If the Ru–O bond is taken as the z axis for each Ru site, mixing can occur between each set of d_{xz}, d_{yz} orbitals with two π-type p orbitals on the bridging O atom. The result is three sets of bridge-based orbitals. Two are bonding orbitals that are largely p_O in character (π_1^b, π_2^b). Two are nonbonding or slightly antibonding orbitals that are largely $d\pi_{Ru}$ in character (π_1^{nb}, π_2^{nb}). Two are antibonding orbitals that are also largely $d\pi_{Ru}$ in character (π_1^*, π_2^*).

In terms of electron count for a μ-oxo d^5 Ru(III) complex, the occupancy of the bridging orbitals is $(\pi_1^b)^2(\pi_2^b)^2(\pi_1^{nb})^2(\pi_2^{nb})^2$-$(\pi_1^*,\pi_2^*)^2$. A bending along the Ru–O–Ru bonding axis results

(13) Cromer, D. T.; Liberman, D. *J. Chem. Phys.* **1970**, *53*, 1891. Hall, S. R.; Stewart, J. M. *XTAL*, 4th ed.; Crystallography Center, University of Western Australia: Nedlands, Australia, 1987.
(14) (a) Wieghardt, K.; Pohl, K.; Gebert, W. *Angew. Chem., Int. Ed. Engl.* **1983**, *22*, 727. (b) Wieghardt, K.; Bossek, U.; Ventur, D.; Weiss, J. *J. Chem. Soc., Chem. Commun.* **1985**, 347. (c) Armstrong, W. H.; Spool, A.; Papaefthymiou, G. C.; Frankel, R. B.; Lippard, S. J. *J. Am. Chem. Soc.* **1984**, *106*, 3653. (d) Sheats, J. A.; Czernuszewicz, R. S.; Dismukes, G. C.; Rheingold, A. L.; Petrouleas, V.; Stubbe, J.; Armstrong, W. H.; Beer, R. H.; Lippard, S. J. *J. Am. Chem. Soc.* **1987**, *109*, 1435. (e) Köppen, M.; Fresen, G.; Wieghardt, K.; Llusar, R. M.; Nuber, B.; Weiss, J. *Inorg. Chem.* **1988**, *27*, 721. (f) Bushkin, J. S.; Schake, A. R.; Vincent, J. B.; Chang, A. R.; Li, Qiaoying; Huffman, J. C.; Christou, G.; Hendrickson, D. N. *J. Chem. Soc., Chem. Commun.* **1988**, *18*, 701. (g) Sasaki, Y.; Suzuki, M.; Tokiwa, A.; Ebihara, M.; Yamaguchi, T.; Kabuto, C.; Ito, T. *J. Am. Chem. Soc.* **1988**, *110*, 6251.
(15) Mathieson, M. L.; Mellor, D. P.; Stephenson, N. C. *Acta Crystallogr.* **1952**, *5*, 185.

Table IV. Important Molecular Dimensions for a Series of μ-Oxo Compounds and Ions

complex	∠MOM, deg	r_{M-O}, Å[a]	r_{M-M}, Å	r_{M-N}, Å[b]	ref
$[Cl_5Ru(\mu\text{-}O)RuCl_5]^{4-}$	180.0	1.87	3.74		15
$[(NH_3)_5Ru(\mu\text{-}O)Ru(en)_2(\mu\text{-}O)Ru(NH_3)_5]^{6+}$ [d]	177.2 (4)	1.87 (4)[e]	3.739 (4)	2.115 (7)–2.151 (6)	4b
$[(bpy)_2(H_2O)Ru(\mu\text{-}O)Ru(H_2O)(bpy)_2]^{4+}$ [d]	165.4 (3)	1.869 (1)	3.71 (4)	2.029 (5)–2.089 (4)	2b
$[(bpy)_2(NO_2)Ru(\mu\text{-}O)Ru(NO_2)(bpy)_2]^{2+}$ [d]	157.2 (3)	1.883 (7)[e]	3.692 (1)	2.034 (8)–2.100 (7)	2a
$[(tpm)Ru(\mu\text{-}O)(\mu\text{-}O_2P(O)(OH))_2Ru(tpm)]$	124.6 (8)	1.870 (15)	3.312 (3)	2.031 (13)–2.147 (25)	c
$[Ru_3(\mu_3\text{-}O)(\mu\text{-}O_2CCH_3)_6(PPh_3)_3]$	119.9 (8)[e]	1.92 (2)[e]	3.329 (3)[e]		3a
$[(tpb)Mn(\mu\text{-}O)(\mu\text{-}O_2CCH_3)_2Mn(tpb)]$ [d]	125.1 (1)	1.773 (2)	3.159 (1)	2.067 (2)–2.196 (3)	14d
$[(tacn)Mn(\mu\text{-}O)(\mu\text{-}O_2CCH_3)_2Mn(tacn)]^{2+}$ [d]	117.9 (2)	1.80 (1)	3.084 (3)	2.06 (1)–2.25 (2)	14b
$[(tacn)Fe(\mu\text{-}O)(\mu\text{-}O_2CCH_3)_2Fe(tacn)]^{2+}$ [d]	123.6 (1)	1.784 (2)[e]	3.1457 (6)	2.148 (3)–2.200 (3)	14c
$[(tacn)Fe(\mu\text{-}O)(\mu\text{-}O_2CCH_3)_2Fe(tacn)]^{2+}$ [d]	117.3 (2)	1.78 (1)[e]	3.064 (5)	2.16 (1)–2.21 (2)	14a
$[(tacn)V(\mu\text{-}O)(\mu\text{-}O_2CCH_3)_2V(tacn)]^{2+}$ [d]	130.2 (2)	1.791 (4)[e]	3.250 (2)	2.152 (5)–2.238 (5)	14e
$[(PPh_3)Cl_2Os(\mu\text{-}O)(\mu\text{-}O_2CCH_3)_2OsCl_2(PPh_3)]$	140.2 (4)	1.829 (10)[e]	3.440 (2)		16
$[(py)_3Ru(\mu\text{-}O)(\mu\text{-}O_2CCH_3)_2Ru(py)_3]^{2+}$	122.2 (5)	1.857 (9)	3.251 (2)	2.072 (10)–2.208 (11)	14g

[a] Metal–oxo bridge distance. [b] Shortest and longest M–N distances. [c] This work. [d] en is an abbreviation for ethylenediamine, bpy for 2,2′-bipyridine, py for pyridine, tpb for the tris(1-pyrazolyl)borate anion, and tacn for 1,4,7-triazacyclononane. [e] Average value.

in a further increase in the energy separation between π_1^*, π_2^* and a further electronic stabilization arising from the double occupation of π_1^*. For the hydrogen phosphato μ-oxo complex, the bending, and therefore the splitting, between π_1^* and π_2^* must be large. The ^1H NMR spectrum of the dimer is consistent with diamagnetism at room temperature with no sign of contribution from a low-lying paramagnetic state. The diamagnetism is consistent with the configuration $(\pi_1^*)^2$ in the ground state. For the μ-oxo bpy ions $[(bpy)_2(L)RuORu(L)(bpy)_2]^{n+}$ (L = H_2O, n = 4; L = NO_2, n = 2), the bending along the Ru–O–Ru axis is limited by bpy-bpy ring contacts. The aqua ion with ∠RuORu = 152.2° is paramagnetic at room temperature but with a singlet ground state consistent with a relatively small splitting between states having the configurations $(\pi_1^*)^2$ and $(\pi_1^*)^1(\pi_2^*)^1$. In the d^4–d^4 ion $Cl_5Ru^{IV}ORu^{IV}Cl_5^{4-}$, there is no occupancy of π_1^*, π_2^* and the Ru–O–Ru bond angle is 180°, which is predicted by the π-bonding model. The π-bonding model successfully predicts the bending along the Ru–O–Ru bridge.

A series of related structures of this kind is known. The examples are based on acetate as a bridging ligand and the monodentate pyridine ligand or the tridentate facial ligands tris(1-pyrazoyl)borate anion and 1,4,7-triazacyclononane. Examples are known for d^5 (Fe^{III}), d^4 (Mn^{III}), d^2 (V^{III}), and d^5 (Ru^{III}). Some of the details of their structures are also summarized in Table IV. In all cases the M–O–M angles are nearly 120°, except for the vanadium case, where the angle is 130°. For the d^4 Os(IV) dimer $[(PPh_3)(Cl)_2Os(\mu\text{-}O)(\mu\text{-}O_2CCH_3)_2Os(Cl)_2(PPh_3)]$[16] the structure is constrained to be bent along the Os–O–Os axis because of the structural demands imposed by the three bridges. The Os–O–Os angle is 140.2° and considerably larger than 120° due to triphenylphosphine–acetate repulsions.

In the hydrogen phosphato complex **1**, the average Ru–O distance in the RuOP(O)(OH)ORu bridging groups is 2.02 Å, while the Ru–O distance for the Ru–O–Ru core is 1.87 Å. The Ru–O bond distances at the bridge are similar to those found in related complexes (±0.02 Å), including $[(bpy)_2(X)RuORu(X)(bpy)_2]^{4+}$ (X = NO_2^-, H_2O), $[Cl_5RuORuCl_5]^{4-}$, and $[(py)_3Ru(\mu\text{-}O)(\mu\text{-}CH_3COO)_2Ru(py)_3]^{2+}$. The relatively short Ru–O bond lengths are consistent with multiple Ru–O bond character, which also is predicted by the π-bonding model.

When the Ru–N bond distance trans to the μ-oxo group is excluded, the average Ru–N bond distance in **1** is 2.04 Å. This is very close to the Ru–N distance found in the $[(py)_3Ru(\mu\text{-}O)(\mu\text{-}CH_3COO)_2Ru(py)_3]^{2+}$ cation and in both the aqua and nitro bpy μ-oxo ions (2.08, 2.05, and 2.07 Å, respectively). The structural impact of strong Ru–O–Ru coupling appears in the hydrogen phosphato dimer **1**, in the long Ru–N bond distance (2.147 Å) for the N atoms trans to the Ru–O–Ru bridge. The differences between the cis and the trans Ru–N bond distances with regard to the bridge are Δr = 0.10 Å for **1**, Δr = 0.13 Å for $[(py)_3Ru(\mu\text{-}O)(\mu\text{-}O_2CCH_3)_2)Ru(py)_3]^{2+}$, and Δr = 0.04 and 0.03 Å for the aqua and nitro bpy (μ-oxo)ruthenium complexes, respectively.

The impact of the increased electron density arising from multiple bonding with the μ-oxo group is also seen in the coordination geometry around the Ru(III) ions. In **1** the octahedral array of atoms coordinating the ruthenium metal ions is distorted. The trans L–Ru–L angles range from 169.7 to 176.5°, indicating only slight distortions from rectilinear geometry. The distortions are systematically away from the μ-oxo Ru–O bond because of the increased electron–electron repulsions associated with the multiple bonding. The three N–Ru–N angles range from 86.4 to 87.2° while the three O–Ru–O angles range from 89.4 to 96.4°. The N–Ru–N angles are constrained by the tpm ligand as expected.

In the bridging $[O_2P(O)(OH)]^{2-}$ ligand the geometry can be described as a distorted tetrahedron around the phosphorus atom with internal angles ranging from 113.8 to 105.0°. The hydrogen is presumably bound to O(3) since the P–O(3) distance is longer by ~0.02 Å than the bond distance of P–O(4). It is possible that the hydrogen might be shared by both oxygen atoms. No significant differences exist in the molecular dimensions of the tpm ligand found here and those described previously in the complex $[Au(CH_3)_2(tpm)](NO_3)$.[17]

Spectral Properties and Redox Chemistry. The ^1H NMR spectra of the triply bridged complexes **1** and **2** were recorded in D_2O, while that of the (acetato)(μ-oxo)ruthenium complex **3** was recorded in acetone-d_6. By utilizing the high symmetry of the compounds, the magnitudes of the coupling constants, and the results of integration experiments, it is possible to assign all the resonances in the spectra. The ^1H NMR spectral assignments for the three complexes are summarized in the Experimental Section according to the labeling scheme shown in Figure 1. A resonance for H10, the hydrogen atom bonded to the bridging carbon atom, is not observed in the spectra of the complexes **1** and **2** in D_2O due to a fast exchange process with the solvent. Nevertheless, for the acetato complex **3** in acetone-d_6, a sharp singlet at 10.8 ppm appears, which can be assigned to this resonance. Because of the difference in electrostatic effects of the phosphato and carbonato ligands compared to that of the acetato ligand, the tpm protons of the complexes **1** and **2** are shielded by 0.2–0.6 ppm compared to the tpm protons of the complex **3**.

The similarity in the patterns of ^1H NMR spectra among the three complexes **1**–**3** suggests that in all cases they share a common structure with the arrangement of atoms at the Ru–O–Ru core closely related. In all cases there is no sign of paramagnetism in the ^1H NMR spectra, and by inference, the complexes are diamagnetic. The diamagnetism is consistent with the considerable bending of the Ru–O–Ru bond axis away from 180° as discussed in the previous section.

The electrochemistry of the three triply bridged ruthenium complexes involving bridging hydrogen phosphate (**1**), carbonate

(16) Armstrong, J. E.; Robinson, W. R.; Walton, R. A. *Inorg. Chem.* **1983**, *22*, 1301.

(17) Canty, A. J.; Minchin, N. J.; Healy, P. C.; White, A. H. *J. Chem. Soc., Dalton Trans.* **1982**, 1795.

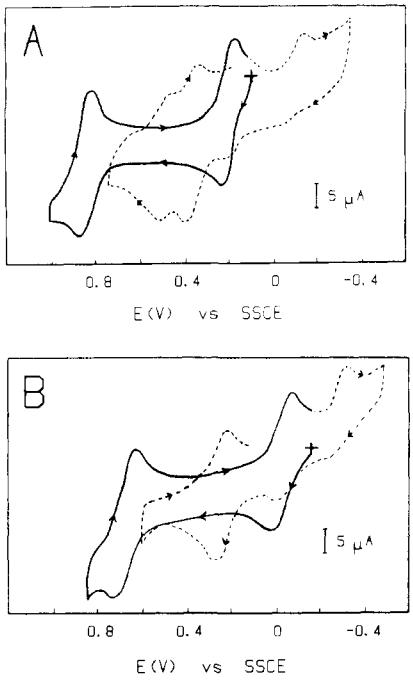

Figure 2. Cyclic voltammograms (vs SSCE at μ = 0.1 M) of [(tpm)-Ru(μ-O)(μ-O_2P(O)(OH))$_2$Ru(tpm)] at a scan rate of 100 mV/s with a glassy-carbon disk (1.5-mm radius) as a working electrode: (A) 0.1 M triflic acid, pH = 1; (B) 0.1 M phosphate buffer, pH = 4.9. The solid line represents the first scan, while the dashed line corresponds to the second scan.

Table V. $E_{1/2}$ Values (vs SSCE at μ = 0.1 M) and Visible Absorption Spectral Features[a]

complex	$E_{1/2}$, V III,IV/ III,III	III,III/ III,II	III,II/ II,II	γ_{max}, nm (log ϵ)
[(tpm)Ru(μ-O)-(O_2P(O)(OH)$_2$)Ru(tpm)]	0.60	−0.13	−0.39[b]	574 (4.21)
[(tpm)Ru(μ-O)-(μ-O_2CO)$_2$Ru(tpm)]	0.71	−0.63[b,c]		572 (4.08)
[(tpm)Ru(μ-O)-(μ-O_2CCH$_3$)$_2$Ru(tpm)]$^{2+}$	1.07	−0.10	−0.25	576 (4.16)

[a] In 0.1 M H_2PO_4/HPO_4^{2-} phosphate buffer solution at pH = 7. [b] This value is the cathodic peak potential, $E_{p,c}$, for a reductive sweep obtained by cyclic voltammetry. The reduction is chemically irreversible. [c] Two-electron wave

(**2**), and acetate (**3**) in aqueous solution provides evidence for the presence of both oxidative and reductive processes within the solvent limits. However, the redox chemistry of the μ-oxo complexes is complicated both by chemically irreversible reduction processes and by pH effects. Cyclic voltammograms of the hydrogen phosphato dimer **1** in aqueous solution at pH 1.0 and at pH 4.9 are shown in Figure 2. The $E_{1/2}$ values obtained vs SSCE at pH 7.0 and visible absorption maxima values λ_{max} at the same pH for the three complexes are collected in Table V.

Visible spectra of the hydrogen phosphato complex over an extended pH range show variations with pH that are attributable to proton gain or loss (Figure 3A). The origins of pH-dependent shifts appear to be through acid–base equilibria at the bridging anion or at the bridging oxo group as in reactions 2 and 3.

$$[(tpm)Ru(\mu\text{-}OH)(\mu\text{-}O_2P(O)(OH))_2Ru(tpm)]^+ \rightleftharpoons [(tpm)Ru(\mu\text{-}O)(\mu\text{-}O_2P(O)(OH))_2Ru(tpm)] + H^+ \quad (2)$$

$$[(tpm)Ru(\mu\text{-}O)(\mu\text{-}O_2P(O)(OH))_2Ru(tpm)] \rightleftharpoons [(tpm)Ru(\mu\text{-}O)(\mu\text{-}O_2P(O)(OH))(\mu\text{-}O_2P(O)_2)Ru(tpm)]^- + H^+ \quad (3)$$

Spectrophotometric titrations of the hydrogen phosphato complex **1** by using limiting molar extinction coefficients in the different pH regions of Figure 3A gave pK_a = 4.62 for reaction 2 (note

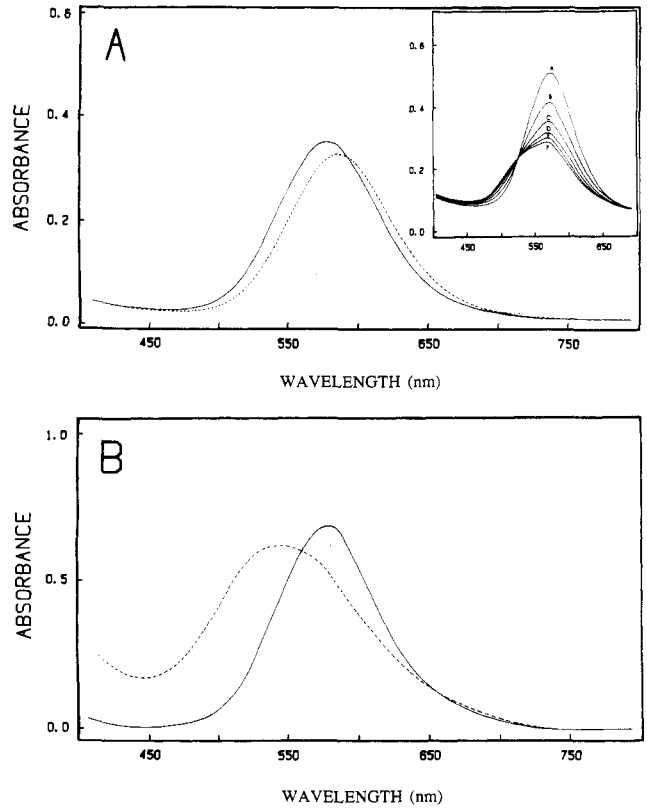

Figure 3. (A) UV–visible spectra of the hydrogen phosphato bridged complex **1** at pH = 1.1 (···), at pH = 7.0 (—), and at pH = 10.7 (- - -). The spectrophotometric titration of [(tpm)Ru(μ-O)(μ-O_2P(O)-(OH))$_2$Ru(tpm)] is shown as an inset (initial [**1**] = 32.22 μM, 1-cm quartz cell, T = 295 K): (a) pH = 6.3; (b) pH = 4.8; (c) pH = 4.3; (d) pH = 3.9; (e) pH = 3.8; (f) pH = 3.5. (B) UV–visible spectra of [(tpm)Ru^{III}(μ-O)(μ-O_2P(O)(OH))$_2$$Ru^{III}$(tpm)] and of [(tpm)$Ru^{III}$($\mu$-O)($\mu$-$O_2$P(O)(OH))$_2$$Ru^{IV}$(tpm)]$^+$ generated by Br_2 oxidation, at pH = 7.0 in 0.1 M phosphate ($H_2PO_4^-/HPO_4^{2-}$) buffer solution.

the data in the inset in Figure 3A) and pK_a = 7.71 for reaction 3, both at μ = 0.1 M and at T = 295 K.

The suggestion that the protonation equilibrium in reaction 2 involves the bridging O atom follows from the recent work of Wieghardt et al. on the closely related complex [(tacn)Ru(μ-O)(μ-O_2CCH$_3$)$_2$Ru(tacn)]$^{2+}$ (tacn is 1,4,7-triazacyclononane).[18] In this complex protonation occurs at the μ-oxo group. The resulting acid has pK_a = 1.9 at 20 °C. The different magnitudes of the spectral shifts in Figure 3A are consistent with different sites of protonation. The intense bands in the visible region have been assigned to Ru–O–Ru bridge-based transitions.[5a,c] The large shift in acidic solution is consistent with a significant electronic perturbation at the bridge caused by protonation.

In the cyclic voltammogram of **1** at pH 1.0 in 0.1 M CF_3SO_3H (Figure 2A), a 1e reversible wave appears at +0.84 V in which the Ru(III)–Ru(III) complex is oxidized to Ru(IV)–Ru(III). Although oxidation-state labels like IV and III are used for convenience, the available evidence suggests that strong electron coupling exists in oxo-bridged dimers. The mixed-valence forms are probably delocalized, and a more appropriate description may be Ru(III.5)–Ru(III.5). The attempted determination of n by coulometry at E_{app} = 1.0 V was unsuccessful because of extended current–time profiles arising from an electrocatalyzed oxidation whose origin we have been unable to establish. The same observations were made by using bromine as the oxidizing agent. Following oxidation to the IV,III ion, return to the III,III form was observed to occur within a few minutes by spectral monitoring.

A second, nearly electrochemically reversible wave appears at 0.2 V (Figure 2A). It is a one-electron reduction to give the III,II form of the complex. However, on the longer time scale of

(18) Neubold, P.; Wieghardt, K.; Nuber, B.; Weiss, J. *Angew. Chem.* **1989**, *100*, 990.

coulometry the III,II ion is unstable (see below). At a scan rate of 100 mV/s the peak to peak splitting, $E_{p,a} - E_{p,c}$, in the cyclic voltammogram is 65 mV.

At pH = 1.0 a second reduction wave at −0.12 V is observed for the hydrogen phosphato complex **1**. The wave corresponds to a second one-electron reduction, III,II + e^- → II,II. In acidic solution, the Ru(II)–Ru(II) complex is unstable even on the cyclic voltammetric time scale. The same pattern of reductive instability has been reported for several μ-oxo complexes of ruthenium.[2b,4c,5] It has been attributed to the fact that reduction occurs at levels (π_1^*, π_2^*) that have antibonding character with regard to the Ru–O–Ru bridge. Once these levels are fully populated, there is no longer a basis for a π-interaction across the bridge leading to a loss in electronic stabilization and the labilization of the bridge.

In the case of the hydrogen phosphato complex, reductive cleavage initially leads to two new species having reversible couples at $E_{1/2}$ = +0.37 and 0.50 V. The point is illustrated in Figure 2A, where the appearance of the two new waves following an initial reductive scan is shown. The wave at $E_{1/2}$ = 0.50 V coincides exactly with $E_{1/2}$ for the Ru(III/II) couple of the complex $[(tpm)Ru(H_2O)_3]^{2+}$. The second couple that appears at $E_{1/2}$ = 0.37 V arises from an intermediate couple in which one of the phosphato ligands is retained. Over a period of minutes the wave at $E_{1/2}$ = 0.37 V loses peak current as the intermediate undergoes aquation to give the aqua couple at 0.50 V.

Coulometric reduction of **1** at E_{app} = −0.20 V and pH = 1 occurs with n = 1.9 to give $[(tpm)Ru(H_2O)_3]^{2+}$ quantitatively. The n value of 1.9 for reduction of the ligand-bridged complex and the nearly doubled peak current for the couples involving the triaqua product compared to the initial complex both corroborate the one-electron nature of the redox processes observed for the initial bridged complex.

A comparison between cyclic voltammograms for the hydrogen phosphato complex at pH = 4.9 and pH = 1.0 shows that the IV,III/III,III couple (at 0.68 V) and the III,III/III,II couple (at 0.07 V) are both pH dependent as expected, given the acid–base equilibria in reactions 2 and 3. An initial reductive scan at pH 4.9 results in an enhancement of the peak height for the phosphate-containing intermediate at the expense of the triaqua couple. In the absence of added phosphate buffer, e.g., in the presence of a phthalate buffer at the same pH, or with a decrease in the scan rate of the cyclic voltammogram the triaqua product is favored. All of our observations are consistent with initial reductive cleavage of the μ-oxo complex but with retention of the phosphato ligand. The first step is followed by loss of the phosphato ligand to give $[(tpm)Ru(H_2O)_3]^{2+}$ in a reaction or reactions that are acid-catalyzed (reactions 4 and 5 at pH = 7.0).

$$[(tpm)Ru^{III}(\mu\text{-}O)(\mu\text{-}O_2P(OH)(O))_2Ru^{III}(tpm)] \xrightarrow{+2e^-} \text{"I"} \quad (4)$$

$$\text{"I"} \rightarrow 2[(tpm)Ru^{II}(H_2O)_3]^{2+} + 2HPO_4^- \quad (5)$$

Cyclic voltammetry at pH = 7 in a μ = 0.1 M phosphate buffer solution for the (carbonato)(μ-oxo)ruthenium complex **2** shows the presence of two redox processes. One is a quasireversible oxidation ($E_{p,a} - E_{p,c}$ = 160 mV) at $E_{1/2}$ = 0.71 V, which is a one-electron process. The other is a chemically irreversible reduction at $E_{p,c}$ = −0.63 V, which is a two-electron process. Coulometric reduction of **2** at E_{app} = 0.75 V occurs with n = 1.8 to give $[(tpm)Ru^{II}(H_2O)_3]^{2+}$ quantitatively.

Cyclic voltammograms of the carbonato complex are pH independent in the range 3.5–12. If the pH is decreased below pH ≈ 3.5, the loss of CO_3^{2-} as CO_2 occurs as revealed by IR spectroscopy. A broad band at 1512 cm^{-1}, assigned to the carbonyl group of the carbonato bridging ligand, disappears under these conditions. The resulting product is presumably the corresponding tetraaqua(μ-oxo)ruthenium complex formed as in reaction 6. Its redox properties are currently under investigation.

$$[(tpm)Ru^{III}(\mu\text{-}O)(\mu\text{-}O_2C(O))_2Ru^{III}(tpm)] + 2H_2O + 4H^+ \rightarrow [(tpm)(H_2O)_2Ru^{III}(\mu\text{-}O)Ru^{III}(H_2O)_2(tpm)]^{4+} + 2CO_2 \quad (6)$$

Cyclic voltammetry at pH = 7 in a μ = 0.1 M phosphate buffer solution for the (acetato)(μ-oxo)ruthenium complex **3** provides evidence for three different redox processes. A quasireversible oxidation wave ($E_{p,a} - E_{p,c}$ = 140 mV) appears at $E_{1/2}$ = 1.07 V, which is a one-electron process. A one-electron quasireversible reduction ($E_{p,a} - E_{p,c}$ = 120 mV) appears at $E_{1/2}$ = −0.10 V. A second quasireversible reduction ($E_{p,a} - E_{p,c}$ = 80 mV) appears at $E_{1/2}$ = −0.25 V.

$E_{1/2}$ values for the hydrogen phosphato and carbonato based III,IV/III,III couples are lower than for the acetato complex by 300–400 mV (Table V). This is, no doubt, a consequence of the differences in charge types of the couples involved and of the enhanced electron-donating ability of the dianionic HPO_4^{2-} and CO_3^{2-} ligands. The enhanced electron-donating capability of the dianions may also play a role in explaining why the II,II forms are unstable on the cyclic voltammetric time scale while two quasireversible reductions are observed for the acetato complex.

Acknowledgments are made to the National Science Foundation under Grant No. CHE-8601604 and the National Institutes of Health under Grant No. GM32296 for support of this research. A.L. acknowledges fellowship support from Fulbright "La Caixa" (Barcelona, Spain). We offer special thanks to Judith Konnert of the U.S. Geological Survey for her assistance in applying the XTAL crystallographic software. We also thank Professor Karl Wieghardt for bringing his work to our attention and for pointing out that the site of protonation in the hydrogen phosphato dimer is probably at the μ-oxo group.

Supplementary Material Available: A listing of anisotropic thermal parameters for non-hydrogen atoms (1 page); a listing of observed and calculated structure factors (9 pages). Ordering information is given on any current masthead page.